nature nanotechnology

SUPPLEMENTARY INFORMATION

DOI: 10.1038/NNANO.2010.84

Hybrid superconductor-semiconductor devices made from self-assembled SiGe nanocrystals on silicon

G. Katsaros, P. Spathis, M. Stoffel, F. Fournel, M. Mongillo, V. Bouchiat, F. Lefloch, A. Rastelli, O. G. Schmidt, S. De Franceschi

This pdf file contains:

Supplementary text

Supplementary figure

References

DOI: 10.1038/NNANO.2010.84

1. Fabrication of ad-hoc silicon on insulator (SOI) substrates

Commercial 200-mm-diameter SOI wafers with a Si upper layer of 70 nm, a Si oxide layer of 145 nm (box layer), and a 0.5-mm-thick undoped Si substrate (handle layer), were thermally oxidized and bonded by means of hydrophilic molecular bonding to a heavily doped Si wafer (resistivity of 0.006-0.010 $Ohm.cm^{-1}$). The SOI handle layer was then removed by grinding and selective chemical etching with a 25% diluted solution of tetramethyl ammonium hydroxide (TMAH) at 75°C. Finally, also the box oxide layer of the original SOI wafer was removed using a 10% fluorhydric acid solution. The final result consisted of non standard SOI substrate having 40-nm-thick Si upper layer, a 65-nm-thick oxide layer (obtained by partial thermal oxidation of the Si upper layer in the original SOI wafer) and a degenerately doped Si substrate.

2. Growth of SiGe self-assembled nanocrystals

The SiGe nanocrystals were grown by solid-source molecular beam epitaxy (MBE) on the SOI substrate described above. After ex-situ chemical cleaning, an additional HF dip was performed to remove the surface oxide. The sample was then transferred into the MBE chamber and outgassed at 620°C prior to the deposition of a 100-nm-thick undoped Si buffer at a rate of 0.1 nm/s. After a 5 s growth interruption, 7 monolayers (ML) of Ge were deposited at 620°C at a rate of 0.04 ML/s. The sample was then cooled down to 300°C and capped with a 2-nm-thick Si layer. Within these growth conditions, the island shape is

preserved[1,2]. These growth conditions yield randomly arranged SiGe nanocrystals with monocrystalline, dome-shaped structure, and rather homogeneous size. From analysis of atomic force microscopy (AFM) images we have obtained a height of: 22±0.8 nm and a base diameter of 96±2 nm. It is known that AFM images overestimate the base diameter. From the SEM images we have estimated the real value of the base diameter to be about 80 nm.

The ordered SiGe dots shown in Fig. 1a were grown onto a Si(001) wafer on which prior to growth a two-dimensional array of holes has been patterned by e-beam lithography and reactive ion etching using a CHF_3/O_2 plasma[3].

3. Device fabrication

InAs self-assembled nanocrystals have been recently used for the realization of electronic devices with either vertical[4-6] or parallel geometry[7-10]. Inspired by the latter works, we have developed a process to fabricate single-hole transistors based on individual SiGe self-assembled nanocrystals.

The fabrication of SiGe quantum-dot devices was accomplished through four steps of e-beam lithography, e-beam metal deposition, and lift-off. In particular, 1) Ti/Au (10/65 nm) bonding pads, 2) an array of NxM pairs of Ti/Au (2/8 nm) linking pads distributed over a 250x250 μm^2 area, 3) an array of NxM pairs of Al (20 nm) electrodes partially overlapping the linking pads and forming gaps of 10-50 nm, and 4) Ti/Au (10/65 nm) electrodes connecting selected pairs of linking pads to the outer bonding pads. In step 3, a 10-15 sec dip in buffered HF was performed prior to Al deposition in order to remove the surface native oxide. Between steps 3 and 4, scanning electron microscopy was used to identify the electrode pairs with a single SiGe nanocrystal.

DOI: 10.1038/NNANO.2010.84

4. Superconductivity-related effects

Bulk aluminium is a conventional superconductor with superconducting critical temperature, T_C = 1.2 K, and superconducting gap Δ = 180 μeV. These values are known to increase in thin films[11]. Consistent with this trend we find Δ = 215 μeV at zero magnetic field and T = 15 mK. This value is extracted from the bias-width of the currentless window around zero bias (Fig. 3c). The currentless window is due to the superconducting nature of the Al electrodes, and to the consequent suppression of quasiparticle transport for V_{SD} between -2Δ/e and 2Δ/e, where Δ is the superconducting energy gap. Following the appearance of this currentless window, all step-like features in the source-drain current are shifted to higher voltages by exactly 2Δ/e. In addition, steps are transformed into asymmetric peaks reflecting the gap-edge singularities in the density of states of the electrodes[12,13].

We consider now the case of cotunnelling transport in the Coulomb blockade regime. In the normal state, elastic cotunnelling processes can take place at any source-drain voltage (i.e., also around zero bias) leading to a featureless background in the differential conductance, dI_{SD}/dV_{SD}. In the case of superconducting electrodes, however, these processes are not allowed for $|V_{SD}| < 2\Delta/e$, because they require the transfer of a quasiparticle from the fully occupied band of one contact (below gap) to the empty band of the other contact (above gap), as it shown in Fig. S1b. As a result, the onset of elastic cotunnelling gives rise to dI_{SD}/dV_{SD} peaks at $\pm 2\Delta/e$[14] which reflect the gap-edge singularities in the quasiparticle density of states of the superconducting electrodes. For the same reason, inelastic cotunnelling processes giving rise to dI_{SD}/dV_{SD} steps at $\pm 2\delta/e$ in the normal state (δ is an excitation energy of the quantum dot) result in the appearance of dI_{SD}/dV_{SD} peaks at $\pm (\delta+2\Delta)/e$ as it is depicted in Fig. S1c. Increasing the magnetic field causes the gradual suppression of the

superconducting gap resulting in the observed inward shift of the elastic and inelastic cotunnelling structures (Fig. S1a).

5. g factors in SiGe QDs

In bulk Si, Ge, and Si_xGe_{1-x} compounds the valence-band edge is characterized by a 4-fold degeneracy between the heavy-hole (HH) and light-hole (LH) states at $\mathbf{k} = 0$. This degeneracy is removed by quantum confinement or strain. Depending on the strain sign the HH or the LH states can be lower in energy. For compressing strain, which is the case for the self-assembled nanocrystals, HH states are lower in energy. In a magnetic field, HH states display an anisotropic spin splitting, with $g_\perp = 6\kappa$ and $g_{//} \approx 0$ the g factors along the growth axis and in the quantum-well plane, respectively. Here κ is the so-called Luttinger valence-band parameter. On the other hand, the LH states exhibit an opposite anisotropy, with $g_{//} = 4\kappa$ and $g_\perp = 2\kappa$[15]. The κ parameter is a material-dependent property and it can take either positive or negative values. In particular, $\kappa = 0.42$ in Si and $\kappa = -3.37$ in Ge leading to positive and negative g factors, respectively[16]. In SiGe alloys, the κ parameter takes intermediate values depending on the relative amount of Ge and Si. According to recent calculations[17], κ varies from –0.308 to –1.153 when the Ge content is increased from 60 to 80%; for low Ge contents it changes sign giving $k = 0.019$ for a Ge content of 40% and $k = 0.131$ for a Ge content of 20%.

In quantum dots, hole motion is confined in all directions. This results in the mixing of HH and LH states which can be strongly influenced by the additional presence of strain. It has been theoretically shown[15] that in the case of small, pure Ge self-assembled nanocrystals with pyramidal shape, confinement and compressive strain cause a significant HH-LH splitting.

DOI: 10.1038/NNANO.2010.84

The first confined state, closest to the valence-band edge, has a dominant HH character leading to a large $|g_\perp|$ (~12) and a pronounced anisotropy ($g_\perp/g_{//} \sim 6$).

The |g| factors and anisotropies measured in the present work are smaller due to different reasons: 1) The dome-shaped self-assembled nanocrystals have a bigger size which implies smaller confinement and strain; 2) The investigated nanocrystals do not consist of pure Ge (for the growth conditions used the Ge content is known to be in 50-75% range[18]).

Supplementary Figure 1

Superconductivity of Al electrodes

a, dI_{SD}/dV_{SD} versus $(B_{//},V_{SD})$ for V_G fixed at the position of the blue line in Fig. 5a. The onset of elastic (black arrow) and inelastic (yellow arrow) cotunneling can be observed. **b-c,** Schematic energy diagrams illustrating the onset of elastic cotunneling at $V_{SD} = 2\ \Delta$ and of inelastic cotunneling at $V_{SD} = 2\ \Delta + \delta$, respectively.

References:

1. Rastelli, A., Müller, E., & von Känel, H. Shape preservation of Ge/Si(001) islands during Si capping. *Appl. Phys. Lett.* **80,** 1438-1440 (2002).

2. Stoffel, M., Denker, U., Kar, G. S., Sigg, H., & Schmidt, O. G. Extended wavelength region of self-assembled Ge/Si(001) islands capped with Si at different temperatures. *Appl. Phys. Lett.* **83,** 2910-2912 (2003).

3. Stoffel, M., Rastelli, A., Merdzhanova, T., Kar, G. S. & Schmidt O. G. Morphological evolution and lateral ordering of uniform Si/Ge(001) islands. *Microelectronics Journal* **37**, 1528-1531 (2006).

4. Austing, D. G. et al. Multiple gated InAs dot ensembles, *Appl. Phys. Lett.* **75**, 671-673 (1999).

5. Vdovin, E. E. et at. Imaging the electron wave function in self-assembled quantum dots, *Science* **290**, 122-124 (2000).

6. Hapke-Wurst, I. et al. Magnetic-field-induced singularities in spin-dependent tunneling through InAs quantum dots, *Phys. Rev. B* **62**, 12621 (2000).

7. Jung, M. et al. Lateral electron transport through single self-assembled InAs quantum dots, *Appl. Phys. Lett.* **86**, 033106 (2005).

8. Hamaya, K. et al. Kondo effect in a semiconductor quantum dot coupled to ferromagnetic electrodes, *Appl. Phys. Lett.* **91**, 232105 (2007).

9. Buizert, C., Oiwa, A., Shibata, K., Hirakawa, K. & Tarucha, S. Kondo universal scaling for a quantum dot coupled to superconducting leads. *Phys. Rev. Lett.* **99,** 136806 (2007).

10. Shibata, K., Buizert, C., Oiwa, A., Hirakawa, K. & Tarucha, S. Lateral electron tunneling through single self-assembled InAs quantum dots coupled to superconducting nanogap electrodes. *Appl. Phys. Lett.* **91,** 112102 (2007).

11. Court, N. A., Ferguson, A. J. & Clark, R. G. Energy gap measurement of nanostructured aluminium thin films for single Cooper-pair devices. *Supercond. Sci. Technol.* **21**, 015013 (2008).

12. Ralph, D. C., Black, C. T. & Tinkham, M. Gate-voltage studies of discrete electronic states in aluminium nanoparticles. *Phys. Rev. Lett.* **78**, 4087-4090 (1997).

13. Doh, Y.-J., De Franceschi, S., Bakkers, E. P. A. M. & Kouwenhoven, L. P. Andreev Reflection versus Coulomb Blockade in Hybrid Semiconductor Nanowire Devices. *Nano Lett.* **12,** 4098-4102 (2008).

14. Grove-Rasmussen, K. et al. Superconductivity-enhanced bias spectroscopy in carbon nanotube quantum dots. *Phys. Rev. B* **79,** 134518 (2009).

15. Nenashev, A. V., Dvurechenskii, A. V. & Zinovieva, A. F. Wave functions and g factor of holes in Ge/Si quantum dots. *Phys. Rev. B* **67,** 205301 (2003).

DOI: 10.1038/NNANO.2010.84

16. Fraj, N., Saïdi, I., Ben Radhia, S. & Boujdaria, K. Band parameters of AlAs, Ge and Si in the 34-band k center dot p model. *Semiconductor Science and Technology* **23,** 085006 (2008).

17. Fraj, N., Saïdi, I., Ben Radhia, S. & Boujdaria, K. Band structures of AlAs, GaP, and SiGe alloys: A 30 k x p model. *J. Appl. Phys.* **102,** 053703 (2007).

18. Stangl, J. et al. Structural properties of semiconductor nanostructures from x-ray scattering. *Advances in Solid State Physics* **44**, 227-238 (2004).

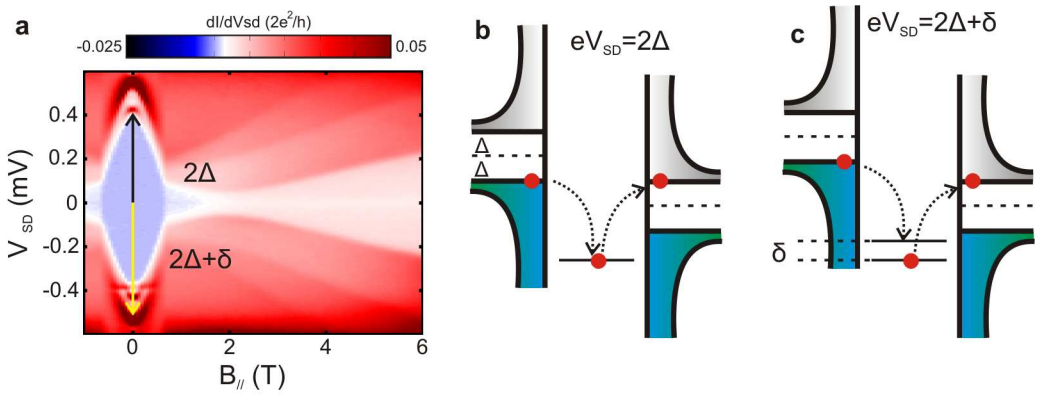

Fig. S1